TURBULENT FRICTION-DRAG REDUCTION CONTROL-SCHEME REQUIRING ONLY STREAMWISE WALL SHEAR SIGNAL

Koji Fukagata, Nobuhide Kasagi
Department of Mechanical Engineering
The University of Tokyo
Hongo, Bunkyo-ku, Tokyo 113-8656, Japan
fukagata@thtlab.t.u-tokyo.ac.jp, kasagi@thtlab.t.u-tokyo.ac.jp

ABSTRACT

We propose a new algebraic control scheme for drag reduction in wall-turbulence, which requires the streamwise wall-shear signal only. By assuming continuously distributed sensors and actuators, the controller is designed to reduce the near-wall Reynolds shear stress that is directly responsible for the turbulent skin friction drag. Intuitive and suboptimal control schemes are considered. The derived control laws are assessed by means of direct numerical simulation of turbulent pipe flow at $Re_\tau \simeq 180$. A clear drag reduction symptom associated with a negative near-wall Reynolds stress is observed when the control scheme derived by the suboptimal control theory is applied.

INTRODUCTION

For successful development of an active feedback control system for drag reduction in wall-bounded turbulent flow, the effectiveness of the control algorithm used as well as the performance of the hardware components such as sensors and actuators is of great importance.

Control schemes may be classified into two types, i.e., *explicit* and *implicit* schemes. The explicit scheme is one in which the control input of the actuator i, ϕ_i, is given explicitly, e.g., $\phi_i(\vec{x},t) = F[s_j(\vec{x},t' \mid t' \le t)]$, where s_j is the sensor information and F is a mapping function. On the other hand, the implicit scheme, such as the optimal control (e.g., Bewley et al., 2001) only describes a relation to be satisfied (i.e. the control input minimizing the cost functional) and requires iterative procedures to determine the control input. While such implicit schemes are useful to explore the possibility of drag reduction control, the explicit schemes are easier to be implemented in the real applications.

In the last decade, various explicit control algorithms were developed and assessed by using direct numerical simulation (DNS) of controlled turbulent flow. Choi et al. (1994) proposed so-called the opposition control, in which blowing/suction velocity is given at the wall so as to oppose the velocity components at a virtual detection plane located above the wall. They attained about 25 % drag reduction in their DNS of turbulent channel flow at low Reynolds numbers. Subsequently, several attempts were made to develop control algorithms using the information measurable at the wall. Lee et al. (1997) used a neural network and obtained an algorithm in which the control input is given as a weighted sum of the spanwise wall-shear stresses, $\partial w/\partial y|_w$, measured around the actuator. Lee et al. (1998) derived series of analytical solutions of the control input to minimize the cost function in the framework of the suboptimal control. Their DNS of channel flow at $Re_\tau \simeq 110$ showed 16-22% drag reduction when $\partial w/\partial y|_w$ (in this case, the control law is quite similar to that obtained by using the neural network mentioned above) or the wall pressure, p_w, was used as the sensor signal.

From a practical point of view, it is desirable to use the streamwise wall-shear stress, $\tau_w = \partial u/\partial y|_w$, or p_w (or both) as a sensor signal because a streamwise wall-shear stress sensor (Yoshino et al., 2003) and a wall pressure sensor (Löfdahl et al., 1996) of sufficiently small size and high frequency response are becoming available. For the use of p_w, in addition to the work by Lee et al. (1998), Koumoutsakos (1999) presented an algorithm to suppress the vorticity flux, and succeeded to reduce the friction drag in his DNS.

For the use of τ_w, however, development of effective algorithm seems more difficult. Lee et al. (1998) also presented a suboptimal solution aiming at reduction of $\overline{\tau_w}$. This algorithm uses τ_w as the sensor signal only, but the friction drag (i.e., $\overline{\tau_w}$) was not reduced by that algorithm. Very recently, Lee et al. (2001) applied a two-dimensional linear-quadratic-Gaussian (LQG) controller to a linearized Navier-Stokes equation. About 10 % drag reduction was attained in their DNS of a channel flow at $Re_\tau \simeq 100$. They also attained 17 % drag reduction by making an *ad hoc* extension. Morimoto et al. (2002) employed a weighted sum of τ_w as the control input and optimized the weights by using the genetic algorithm (GA). The excellent gene (i.e., the pattern of weights) led to 12 % drag reduction in a channel flow at $Re_\tau \simeq 100$.

The previous suboptimal control using the streamwise wall-shear signal only targeted at direct suppression of the streamwise wall-shear. Namely, the cost functional may be expressed as

$$\mathcal{J}(\phi) = \frac{\ell}{2A\Delta t}\int_S\int_t^{t+\Delta t}\phi^2\,dt\,dS + \frac{1}{2A\Delta t}\int_S\int_t^{t+\Delta t}\left(\left.\frac{\partial u}{\partial y}\right|_w\right)^m dt\,dS, \tag{1}$$

where ϕ is control input, which is the blowing/suction velocity and the wall, ℓ represents the price of the control and m is usually chosen as 1 or 2. However, in the framework of suboptimal control, it is not necessary to reduce the streamwise wall-shear at every instance. All we should consider is to modify the flow structure so that the modification leads to a drag reduction in the long run. Therefore, in the present study, we develop control laws in an alternative approach.

THEORETICAL BACKGROUND

Under the condition of constant flow rate, the skin friction drag, $C_f = \overline{\tau_w^*}/[(1/2)\rho^* U_b^{*2}]$, in fully developed channel and pipe flows can be decomposed as

$$C_f = \frac{12}{Re_b} + 12\int_0^1 2(1-y)(-\overline{u'v'})\,dy \tag{2}$$

and

$$C_f = \frac{16}{Re_b} + 16\int_0^1 2r\,\overline{u_r' u_z'}\,r dr, \tag{3}$$

respectively (Fukagata et al., 2002). Here, all variables without superscript are those nondimensionalized by the channel half width, δ^*, or the pipe radius, R^*, and twice the bulk mean velocity, $2U_b^*$, whereas

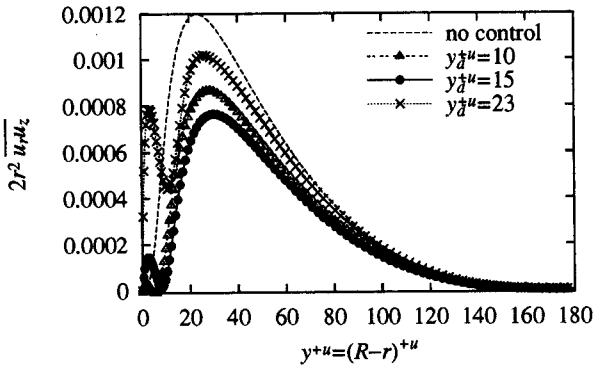

Figure 1: Weighted Reynolds stress distribution of the opposition-controlled flow with different detection plane heights y_d.

dimensional variables are denoted by the superscript of $*$. The bulk Reynolds number is defined as

$$Re_b = \frac{2U_b^*\delta^*}{\nu^*}, \quad \text{or} \quad Re_b = \frac{2U_b^*R^*}{\nu^*}, \tag{4}$$

Equations (2) and (3) indicate that the skin friction coefficient is decomposed into two parts. One is the laminar contribution given by the well-known laminar solution, and the other is the turbulent contribution, which is proportional to the weighted integral of Reynolds shear stress. Figure 1 shows the weighted Reynolds stress appearing in Eq. (3) (i.e., $2r^2\overline{u_r'u_z'}$), in a pipe flow controlled by the opposition control algorithm with different detection plane heights, y_d^{+u}. The difference in the areas covered by the controlled and uncontrolled flow curves is directly proportional to the drag reduction by control. The maximum drag reduction rate is obtained with $y_d^{+u} = 15$. It is clear that most of the drag reduction is attributed to the suppression of near-wall Reynolds stress. As reported in the opposition control of channel flows (Choi et al, 1994; Hammond et al., 1998), the drag reduction rate decreases when too high detection plane is used. This is due to the drastic increase of the Reynolds stress very near the wall, as illustrated for the case of $y_d^{+u} = 23$ in Fig. 1.

Another observation in Fig. 1 is that the Reynolds stress far from the wall is also suppressed, although what is directly suppressed due to the formation of a virtual wall (Hammond et al., 1998) should be the near-wall Reynolds stress only. This can be explained by a gradual outward propagation of the change of Reynolds stress, which happens in the near wall layer. This is similar to the observation in the pipe flow with the opposition control applied partially to wall (Fukagata & Kasagi, 2003). In that simulation, the profile near the wall drastically changes due to the direct suppression at the beginning of controlled region; then, the distribution far from the wall changes gradually following the quick change in the near-wall region. Although the control input in that example is switched on in space, a similar phenomenon is expected when it is turn on at a certain time to a fully developed uncontrolled flow.

CONTROL SCHEME

Intuitive control

The above discussion suggests that suppression of the near-wall Reynolds shear stress is of primary importance in order to reduce the skin friction drag. Once the near-wall Reynolds shear stress is suppressed, its propagation toward the outer layer is also expected to result in an additional drag reduction.

As is well known, the positive Reynolds shear stress (i.e., $-\overline{u'v'} > 0$) near the wall is a consequence of the dominance of the sweep/ejection motions, as shown in the left of Fig. 2. Therefore, an

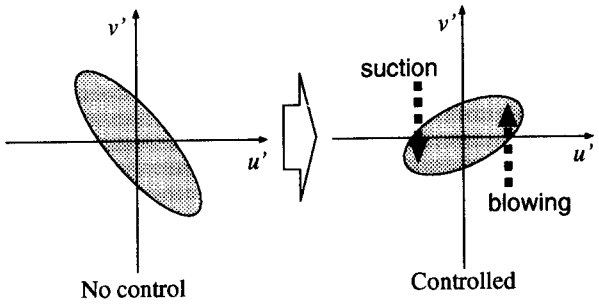

Figure 2: Schematic of the intuitive control scheme.

intuitive control strategy in order to attenuate the Reynolds stress in the vicinity of the wall is to apply blowing to the high-speed region and suction to the low-speed region (see, Fig. 2, right). This can be expressed as

$$\phi = \alpha \left.\frac{\partial u}{\partial y}\right|_w', \quad \text{or} \quad \phi = \alpha \left.\frac{\partial u_z}{\partial r}\right|_w', \tag{5}$$

for a channel or a pipe, respectively. Here, α is the amplitude coefficient and the prime denotes the fluctuation component. Note that the control input is defined as $\phi(x,z,t) = v(x,0,z,t)$ for a channel and $\phi(\theta,z,t) = u_r(1,\theta,z,t)$ for a pipe.

Suboptimal control

Cost functional. A control law can also be derived by using the suboptimal control theory. First, we propose a cost functional $\mathcal{J}$ to be minimized as

$$\mathcal{J}_c(\phi) = \frac{\ell}{2A\Delta t}\int_S\int_t^{t+\Delta t}\phi^2\,dt\,dS + \frac{1}{2A\Delta t}\int_S\int_t^{t+\Delta t}(-u'v')_{y=Y}\,dt\,dS \tag{6}$$

for a channel flow and

$$\mathcal{J}_p(\phi) = \frac{\ell}{A\Delta t}\int_S\int_t^{t+\Delta t}\phi^2\,dt\,dS + \frac{1}{A\Delta t}\int_S\int_t^{t+\Delta t}(u_r'u_z')_{r=(R-Y)}\,dt\,dS \tag{7}$$

for a pipe flow, respectively. Here, ϕ denotes the control input, i.e., the blowing/suction velocity at the wall, A is the area of wall, Δt is the time-span for optimization, and ℓ is the price for the control.

The proposition is to minimize this cost functional under the linearized Navier-Stokes equation. Since a very short time, Δt, is considered here, the linearization is done by neglecting the advection term in the Navier-Stokes equation, similarly to Lee et al. (1998).

Control law for channel flow. At first, a channel flow is considered for simplicity. The Reynolds shear stress above the wall ($y = Y$) is approximated by using the Taylor expansion, i.e.,

$$\left.\begin{aligned} u'(Y) &= Y\left.\frac{\partial u'}{\partial y}\right|_w + O(Y^2) \\ v'(Y) &= \phi + O(Y^2) \end{aligned}\right\} \Longrightarrow -u'v'(Y) = -Y\phi\left.\frac{\partial u'}{\partial y}\right|_w + O(Y^2). \tag{8}$$

Note that the leading term for $v'(Y)$ in the absence of the control input is on the second order. With control, however, the zeroth-order term appears. Substitution of Eq. (8) into Eq. (6) yields an approximated cost functional, i.e.,

$$\mathcal{J}_c(\phi) = \frac{\ell}{2A\Delta t}\int_S\int_t^{t+\Delta t}\phi^2\,dt\,dS - \frac{Y}{2A\Delta t}\int_S\int_t^{t+\Delta t}\phi\left.\frac{\partial u'}{\partial y}\right|_w dt\,dS. \tag{9}$$

The control input, ϕ, that minimize the cost functional, Eq. (9), can be calculated analytically through the procedure proposed by Lee et al. (1998) as follows.

First, the Fréchet differential is applied to the cost functional, i.e.,

$$\frac{\mathcal{D}J_c}{\mathcal{D}\phi}\tilde{\phi} = \frac{\ell}{A\Delta t}\int_S\int_t^{t+\Delta t}\phi\tilde{\phi}\,dt\,dS - \frac{Y}{2A\Delta t}\int_S\int_t^{t+\Delta t}\left(\left.\frac{\partial u}{\partial y}\right|_w\tilde{\phi}+\phi\left.\frac{\partial q}{\partial y}\right|_w\right)dt\,dS\,. \tag{10}$$

Here, the Fréchet differential is defined by

$$\frac{\mathcal{D}f(\phi)}{\mathcal{D}\phi}\tilde{\phi} = \lim_{\varepsilon\to 0}\frac{f(\phi+\varepsilon\tilde{\phi})-f(\phi)}{\varepsilon}\,, \tag{11}$$

and q is the differential state of the streamwise velocity, i.e.,

$$q = \frac{\mathcal{D}u}{\mathcal{D}\phi}\tilde{\phi}\,. \tag{12}$$

Next, a two-dimensional (the streamwise and spanwise) Fourier transform is applied to the approximated cost functional, Eq. (9), to read

$$\widehat{\frac{\mathcal{D}J_c}{\mathcal{D}\phi}}\hat{\tilde{\phi}}^* = \ell\hat{\phi}\hat{\tilde{\phi}}^* - \frac{Y}{2}\left(\left.\widehat{\frac{\partial u}{\partial y}}\right|_w\hat{\tilde{\phi}}^*+\hat{\phi}\left.\widehat{\frac{\partial q}{\partial y}}^*\right|_w\right)\,. \tag{13}$$

where the hat denotes the Fourier component and the subscript of $*$ denotes the complex conjugate.

The modification of the streamwise velocity due to the perturbation field, q, that appears in Eq. (13) can be determined by solving the Fréchet differential of the state equation (i.e., the linearized Navier-Stokes equation). Since here we consider the same state equation and boundary condition ($v_w = \phi$) as those used by Lee et al. (1998), we simply borrow their solution of q that reads

$$\hat{q}(y) = \frac{ik_x}{k}\tilde{\phi}\left(\exp[-(2Re/\Delta t)^{1/2}\,y]-\exp[-ky]\right)\,. \tag{14}$$

Here, k_x is the streamwise wave number and k is the two-dimensional absolute wavenumber, i.e., $k=\sqrt{k_x^2+k_z^2}$. From this solution, the complex conjugate of the wall-shear modification due to the perturbation field can be calculated as

$$\left.\widehat{\frac{\partial q}{\partial y}}^*\right|_w \simeq \sqrt{\frac{2Re}{\Delta t}}\,\frac{ik_x}{k}\,\hat{\tilde{\phi}}^* \tag{15}$$

where the same assumption as that used by Lee et al. (1998), i.e., $k^2 \ll 2Re/\Delta t$ is used.

Finally, by substituting, Eq. (15) into Eq. (13), we can find the suboptimal control input that makes $(\mathcal{D}J_c/\mathcal{D}\phi)\tilde{\phi}=0$ for any $\tilde{\phi}$, as

$$\hat{\phi} = \frac{C}{1/\lambda - ik_x/k}\left.\widehat{\frac{\partial u}{\partial y}}\right|_w\,. \tag{16}$$

There are two parameters in this algorithm:

$$C = \sqrt{\frac{\Delta t}{2Re}} \tag{17}$$

is the amplitude coefficient and

$$\lambda = \frac{Y}{2C\ell} \tag{18}$$

can be interpreted as a length scale as explained below.

Control law for pipe flow. The algorithm for a pipe flow can be developed similarly by using the Taylor expansion of the near-wall Reynolds stress, i.e.,

$$u_r'u_z'(1-Y) = -Y\phi\left.\frac{\partial u_z'}{\partial r}\right|_w + O(Y^2)\,. \tag{19}$$

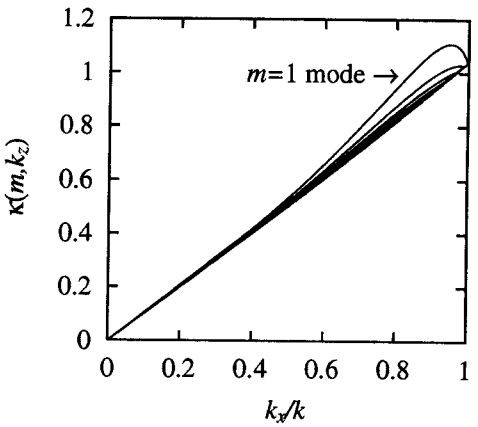

Figure 3: Correlation between k_x/k for channel and $\kappa(m,k_z)$ for pipe.

and the solution of q for pipe flow (Xu et al., 2002), i.e.,

$$\hat{q} = i\widehat{\rho_w}\frac{k_z\Delta t}{2}\left[\frac{I_m(r/C)}{I_m(1/C)}-\frac{I_m(k_z r)}{I_m(k_z)}\right]\,, \tag{20}$$

where

$$\widehat{\rho_w} = -\frac{2}{\Delta t}\left[\frac{I_m(1/C)}{I_{m+1}(1/C)}+\frac{I_m(1/C)}{I_{m-1}(1/C)}\right]\hat{\phi}\Big/k_p\,, \tag{21}$$

and

$$k_p = k_z\left[\frac{I_{m+1}(k_z)}{I_m(k_z)}\frac{I_m(1/C)}{I_{m+1}(1/C)}+\frac{I_{m-1}(k_z)}{I_m(k_z)}\frac{I_m(1/C)}{I_{m-1}(1/C)}-2k_zC\right]\,. \tag{22}$$

Here, m is the azimuthal mode number and $k=\sqrt{k_z^2+m^2}$, and $I_m(r)$ denotes the m-th order modified Bessel function, i.e., $I_m(r) = (-i)^m J_m(ir)$. The length is nondimensionalized by R^*, and hence $k_\theta = (2\pi m)/(2\pi R^*) = m$. The expression above is simplified as compared to the original one by Xu et al. (2002) by this nondimensionalization and by using the similar assumption as that made for channel, i.e., $k_z^2, m^2 \ll 2Re/\Delta t$.

Following the similar procedure as that for the channel flow, we obtain the control input

$$\hat{\phi} = \frac{C}{1/\lambda - i\kappa(m,k_z)}\left.\widehat{\frac{\partial u_z}{\partial r}}\right|_w\,. \tag{23}$$

The difference from the solution for channel flow is absorbed into the factor, $\kappa(m,k_z)$. As can be imagined from Eqs. (20)-(22), the exact expression of $\kappa(m,k_z)$ is highly complicated. However, under the condition of $|m| \ll 1/C$, the asymptotic expression for the modified Bessel function, i.e.,

$$I_m(1/C) \simeq \frac{1}{\sqrt{2\pi/C}}\exp(1/C)\,, \tag{24}$$

simplifies the expression of $\kappa(m,k_z)$, as

$$\kappa(m,k_z) = \left[\left(\frac{C}{2}+1\right)\frac{I_m(k_z)}{I_m'(k_z)}-C\right]\,, \tag{25}$$

where $I_m'(r)$ is the radial derivative of $I_m(r)$. The amplitude parameter, C, is usually much smaller than unity. In that case, Eq. (25), can be further simplified to read

$$\kappa(m,k_z) = \frac{I_m(k_z)}{I_m'(k_z)}\,, \tag{26}$$

The correlation between the wavenumber-dependent parts, i.e., k_x/k for channel and $\kappa(m,k_z)$ for pipe, is shown in Fig. 3. The correlation is nearly linear for higher wave numbers. Naturally, the largest deviation is observed at the lowest azimuthal wavenumber ($m=1$).

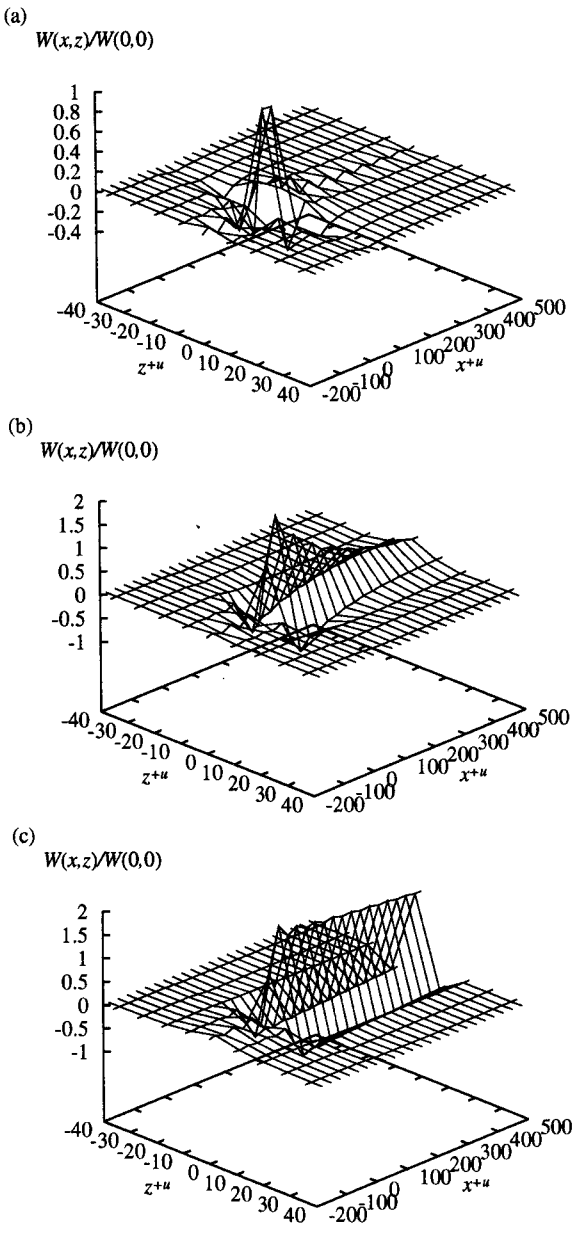

Figure 4: The normalized weights in the physical space: (a) $\lambda = 7$; (b) $\lambda = 73$; (c) $\lambda = 728$. The number of modes is 256 and 128 in the streamwise and spanwise directions, respectively.

Weights in the physical space. The derived control algorithms can be transformed to the physical space through the following inverse Fourier transform:

$$\widehat{\phi} = \widehat{W}^* \left.\frac{\widehat{\partial u}}{\partial y}\right|_w$$

$$\overset{\text{F.T.}}{\Longrightarrow} \quad \phi(x,z) = \int_{-\infty}^{\infty}\int_{-\infty}^{\infty} W(x',z') \left.\frac{\partial u}{\partial y}\right|_w (x+x', x+z')\,dx'dz' \quad , \tag{27}$$

where $\widehat{W}^*$ is the function preceding τ_w in Eqs. (16) and (23). This indicates that the control input of an actuator is given by a weighted integration of τ_w around it. Figure 4 shows the weight, W, in the case where 256 and 128 modes are used in the streamwise and spanwise directions, respectively. The distribution has different characteristics in the streamwise and the spanwise directions. The length scale of the exponential decrease downstream of the actuator is seemingly determined by λ.

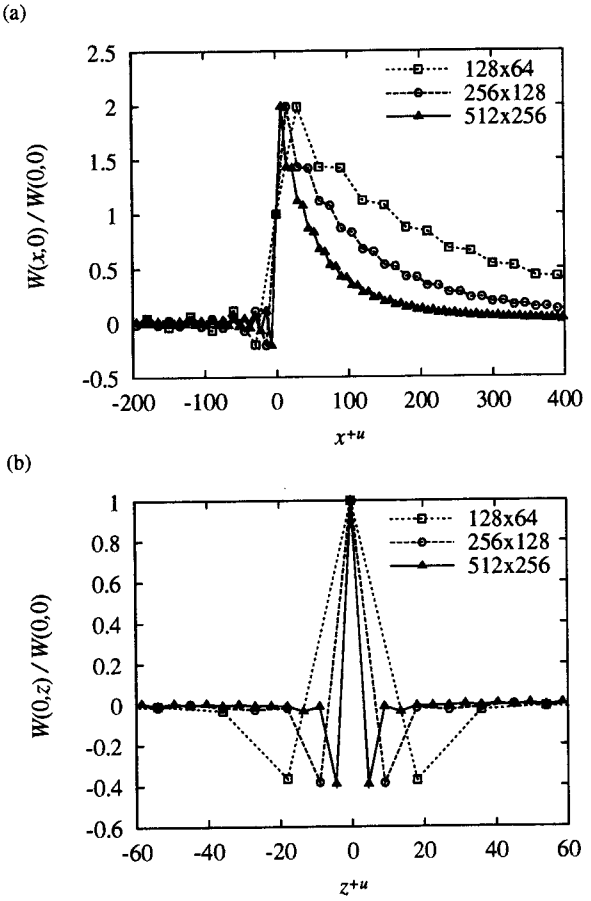

Figure 5: The normalized weights in the physical space ($\lambda = 73$) with different mode numbers. (a) streamwise distribution; (b) spanwise distribution.

In order to investigate on the behavior of the weight in detail, the streamwise distribution in the plane of $z = 0$ and the spanwise distribution in the plane of $x = 0$ are examined by varying the mode numbers used, as depicted in Fig. 5. In both figures, the weights are normalized by $W(0,0)$. Although the distribution in the physical space is dependent on the number of modes used, it is nearly independent of the sensor index. Therefore, the control law is more properly expressed in the discretized space as

$$\phi_{k\ell} = \sum_i \sum_j W_{ij} \left.\frac{\partial u}{\partial y}\right|_{w,\, k+i\, \ell+j} . \tag{28}$$

The values of weights around the actuator for a typical case ($\lambda = 73$) is tabulated in Table 1.

Although the analysis above is made for the case of channel flow, the distribution of the weight for the pipe flow is found to be essentially the same.

PERFORMANCE TEST

Performance of the proposed control algorithm is assessed by DNS of turbulent pipe flow. The DNS code is based on the energy conservative finite difference method for the cylindrical coordinate

Table 1: Normalized weights, W_{ij}/W_{00} around an actuator ($\lambda = 73$).

	$i=-2$	-1	0	1	2	3	4
$j=0$	0.1	-0.2	1.0	2.0	1.4	1.4	1.1
± 1	0.0	0.1	-0.4	-0.7	-0.5	-0.4	-0.3

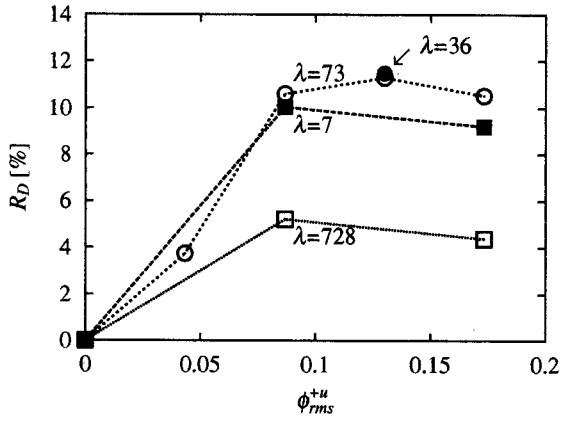

Figure 6: Drag reduction rate, R_D.

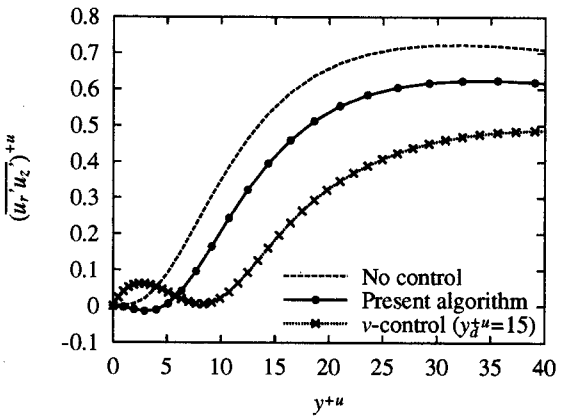

Figure 7: Reynolds stress ($\lambda = 73$, $\phi^{+u}_{rms} = 0.08$).

system (Fukagata & Kasagi, 2002). The time integration is done by using the low storage third-order Runge-Kutta/Crank-Nicolson scheme (Spalart et al., 1991) The bulk mean velocity U_b is kept constant, and the Reynolds number is $Re_b = 5300$ ($Re_\tau = u_\tau^* R^*/\nu^* \simeq 180$ for uncontrolled flow). The computational domain has a longitudinal length of $L = 20R$ and the periodic boundary conditions are applied at both ends. The root mean square of the control input, ϕ_{rms}, is kept constant.

First, the control law derived by using the suboptimal formulation is examined. Figure 6 shows the computed drag reduction rate for different values of λ and ϕ^{+u}_{rms}. Here, the superscript of $+u$ denotes the wall unit of uncontrolled flow. For any values of λ tested here, large drag reduction rate is obtained when ϕ^{+u}_{rms} is of order of 0.1. This amplitude is nearly the same as that of the opposition control with the detection plane height of $y_d^{+u} \simeq 10$. The optimum value of λ seems to be between 10-100.

Figure 7 shows the Reynolds shear stress near the wall. As can be seen, with the present control the near-wall Reynolds stress is suppressed as intended. More interestingly, it takes negative values in the region of $0 < y^{+u} < 5$. As shown in Fig. 8, the joint probability density distribution of the streamwise and wall-normal velocity fluctuations in the near-wall layer ($0 < y^{+u} < 5$) exhibits a similar change to what we initially expected (Fig. 2). The sweeping motion is especially suppressed, whereas the low-speed inward and high-speed outward motions are enhanced by the present control.

These results suggest a possibility of drastic drag reduction even if the near-wall turbulent structure can be manipulated directly — by making a largely negative Reynolds stress in the near-wall layer, or by directly suppressing the Reynolds stress farther from the wall as is the case of the opposition control compared in Fig. 7.

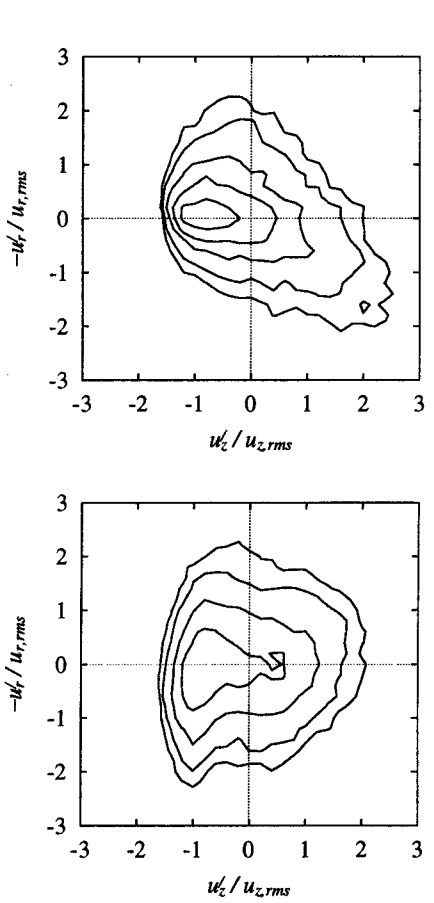

Figure 8: Joint probability density distribution of the streamwise and wall-normal velocity fluctuations in the near-wall layer ($0 < y^{+u} < 5$). (a) No control; (b) Present algorithm. The increment of contours is constant in the logarithmic scale.

For the intuitive control scheme, Eq. (5), the computation is very unstable and drag reduction is not observed with any value of the parameter examined. Such unstable behavior is illustrated in Figure 9. Here, time traces of the control input ϕ of one actuator are plotted for four different control schemes:

1. Reynolds stress-based intuitive control, i.e., Eq. (5);
2. Reynolds stress-based suboptimal control, i.e., Eq. (16);
3. streamwise wall shear-based intuitive control (Lee et al., 1998), i.e.,
$$\hat{\phi} = -i\frac{k_x}{k}\left.\frac{\widehat{\partial u}}{\partial y}\right|_w ; \tag{29}$$
4. spanwise wall shear-based intuitive control (Lee et al., 1998), i.e.,
$$\hat{\phi} = i\frac{k_z}{k}\left.\frac{\widehat{\partial w}}{\partial y}\right|_w . \tag{30}$$

In all cases, the magnitude of control input is fixed at $\phi^{+u}_{rms} = 0.08$. It is clear that two schemes that successfully reduce the drag (i.e., the present $(-uv)$-based suboptimal control law and the $(\partial w/\partial y)$-based suboptimal control law by Lee et al.) give almost constant control input in this short period of time (1 wall unit time), whereas those do not reduce the drag give oscillatory control input. Note that the CFL number in the computation is on order of 0.1 so that this instability is not a purely numerical one. The instability is rather originated from

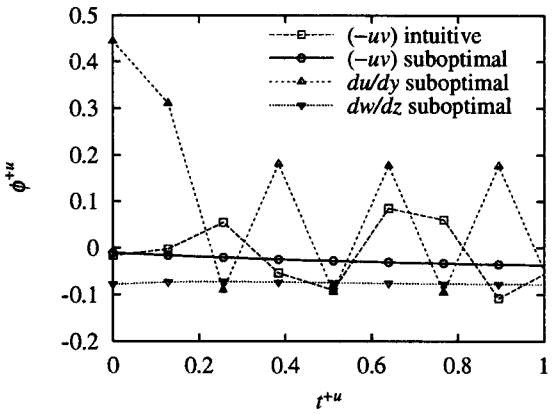

Figure 9: Time trace of control input of an actuator with different control schemes.

the coupling between the dynamics of the plant (i.e., fluid flow) and the controller.

DISCUSSION

It is interesting to investigate why the wall shear-based analytical suboptimal solution, Eq. (29), does not reduce the drag (Lee et al., 1998), while the Reynolds-stress based one in the present study can. Lee et al. (1998) argues that Eq. (29) does not work because the advection term is not at all accounted for. This, however, may not be solely responsible for the failure, because the time domain considered in the suboptimal control is very short so that the advection term can be neglected.

According to the present results, another reason can be pointed out. The cost function by Lee. et al. (1998) directly includes the friction drag, i.e., $(\partial u/\partial y)_w$. This is equivalent, in the framework of the present study, to reduce the second term in Eq. (2), which also includes the contribution of the Reynolds stress far from the wall. However, the modification of flow that can be predictable by the linearized Navier-Stokes equation and the flow that is directly controllable from the wall in a short period are limited near the wall. Namely, the cost functional based on $(\partial u/\partial y)_w$ is contaminated by the unpredictable/uncontrollable information originating far from the wall. The present approach, on the other hand, limits its target to the near-wall Reynolds stress only and the reduction of far-wall Reynolds stress is simply left to the natural secondary effect (Fukagata & Kasagi, 2003). Namely, the cost functional and the derived control law concerns with the predictable/controllable information only. Of course, this argument is valid only for the suboptimal formulation with a linearized Navier-Stokes equation, but not for the optimal formulation that deals with a large spatio-temporal domain.

CONCLUSIONS

Based on the knowledge on the componential contribution to the skin friction (Fukagata et al, 2002), an alternative cost functional for drag reduction, which incorporate the near-wall Reynolds shear stress, was proposed in the framework of the suboptimal control. The control input to minimize that cost functional was analytically obtained by using the method proposed by Lee et al. (1998).

DNS of pipe flow at $Re_\tau \simeq 180$ with the proposed control algorithm showed a clear drag reduction effect. Although the drag reduction rate attained by the present algorithm was small, the result suggests a clue on further drag reduction through manipulation at the wall only.

ACKNOWLEDGMENT

This work was supported through the Project for Organized Research Combination System by the Ministry of Education, Culture, Sports and Technology of Japan (MEXT).

REFERENCES

Bewley, T.R., Moin, P., and Temam, R., 2001. DNS-based predictive control of turbulence: an optimal benchmark for feedback algorithms. *J. Fluid Mech.* **447**, 179-225.

Choi, H., Moin, P. and Kim, J., 1994. Active turbulence control for drag reduction in wall bounded flows. *J. Fluid Mech.* **262**, 75-110.

Endo, T., Kasagi, N., Suzuki, Y., 2000. Feedback control of wall turbulence with wall deformation. *Int. J. Heat Fluid Flow* **21**, 568-575.

Fukagata, K., Iwamoto, K, and Kasagi, N., 2002. Contribution of Reynolds stress distribution to the skin friction in wall-bounded flows. *Phys. Fluids* **14**, L73-L76.

Fukagata, K. and Kasagi, N., 2002. Highly energy-conservative finite difference method for the cylindrical coordinate system. *J. Comput. Phys.* **181**, 478-498.

Fukagata, K. and Kasagi, N., 2003. Drag reduction in turbulent pipe flow with feedback control applied partially to wall. *Int. J. Heat Fluid Flow* **24**, (to appear).

Hammond, E.P., Bewley, T.R., Moin, P., 1998. Observed mechanisms for turbulence attenuation and enhancement in opposition-controlled wall-bounded flows. *Phys. Fluids* **10**, 2421-2423.

Koumoutsakos, P., 1999. Vorticity flux control for a turbulent channel flow. *Phys. Fluids* **11**, 248-250.

Lee, C., Kim, J., Babcock, D., and Goodman, R., 1997. Application of neural networks to turbulence control for drag reduction. *Phys. Fluids* **9**, 1740-1747.

Lee, C., Kim, J. and Choi, H., 1998. Suboptimal control of turbulent channel flow for drag reduction. *J. Fluid Mech.* **358**, 245-258.

Lee., K.H., Cortelezzi, L., Kim, J., and Speyer, J., 2001. Application of reduced-order controller to turbulent flows for drag reduction. *Phys. Fluids* **13**, 1321-1330.

Löfdahl, L., Kälvesten, E., and Stemme, G., 1996. Small silicon pressure transducers for space-time correlation measurements in a flat plate boundary layer. *J. Fluids Eng.* **118**, 457-463.

Morimoto, K., Iwamoto, K., Suzuki, Y., and Kasagi, N., 2002. Genetic algorithm-based optimization of feedback control scheme for wall turbulence. In: *Proc. 3rd Int. Symp. on Smart Control of Turbulence, Tokyo, March 3-5, 2002*, pp. 107-113.

Spalart, P.R., Moser, R.D., Rogers, M.M., 1991. Spectral methods for the Navier-Stokes equations with one infinite and two periodic directions. *J. Comput. Phys.* **96**, 297-324.

Xu, C.-X., Choi, J.-I., Sung H.J., 2002. Suboptimal control for drag reduction in turbulent pipe flow. *Fluid Dyn. Res.* **30**, 217-231.

Yoshino, T., Suzuki, Y., Kasagi, N., and Kamiunten, S., 2003. Optimum design of micro thermal flow sensor and its evaluation in wall shear stress measurement, In: *Proc. IEEE Int. Conf. MEMS'03, Kyoto, Jan. 2003*, pp. 193-196.